Supplementary Information

Neoclassical radial transport coefficients for W7-X limiter magnetic configurations and confinement data

C.D. Beidler, A. Dinklage, G. Fuchert

The normalized mono-energetic radial transport coefficients $D_{11}^{\star}$ for the 'lower-mirror' and 'higher mirror' magnetic configurations calculations with the DKES code at an effective radius of r_{eff} = 6cm are shown in Supplementary Fig. 1 (using the same terminology as in [36]: $\nu^{\star} = (\nu R/(\iota v))$ is the collisionality with the collision frequency ν the major radius R, the rotational transform ι and the particle velocity v).

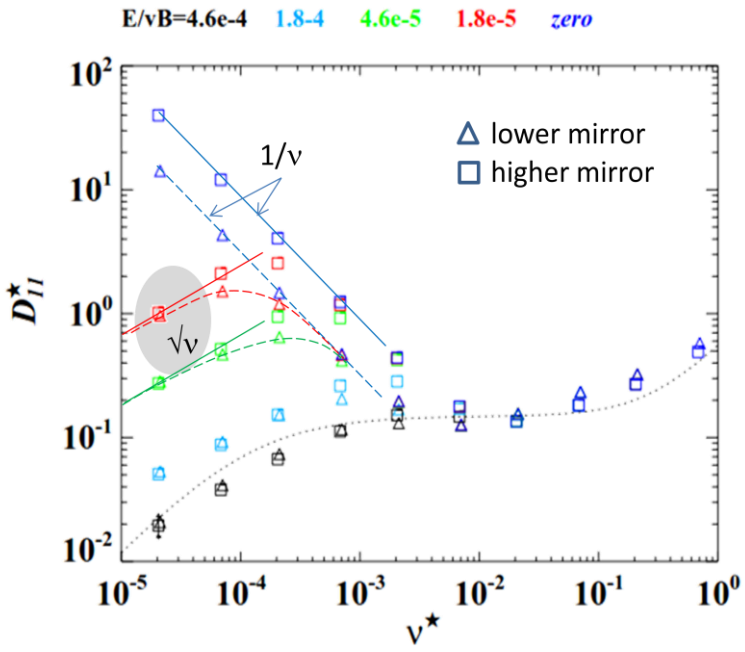

Supplementary Fig. 1| Normalized mono-energetic radial transport coefficient. The transport coefficients $\boldsymbol{D_{11}^{\star}}$ are shown for the higher-mirror (squares) and lower-mirror (triangles) configurations as functions of collisionality and normalized radial electric field at a minor plasma radius of r_{eff} = 6cm. The portion of the plot making the largest contribution to the thermal neoclassical energy transport coefficient for the electrons (largest energy loss channel, see Fig. 6**b** and **e**) at experimental temperatures, densities and radial electric field (Figs. 5, 6**a,d**) is indicated by the gray shaded area.

Supplementary Fig. 1 shows minor differences for the $D_{11}^{\star}$ between the investigated magnetic configurations in the $\sqrt{\nu}$ regime at the collisionalities and electric field values relevant for the experimental conditions in this paper (indicated by the grey shaded area; in order to ease the identification of differences between the configurations, the solid and dashed lines are provided at fixed E_r/vB . Results for $1/\nu$ transport differ by roughly a factor of two, as the E_r/vB =0 results indicate, but such small values of the electric field are of no relevance under electron-root conditions.

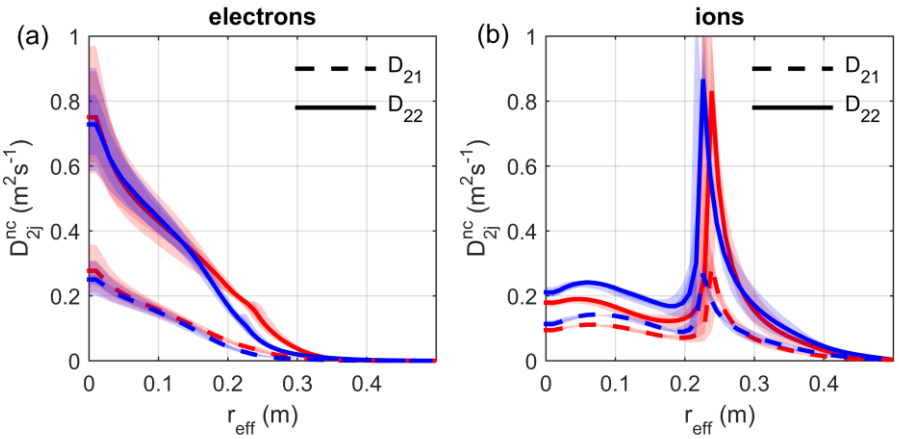

Supplementary Fig. 2| Thermal neoclassical energy transport coefficients. The plots show thermal energy transport coefficient profiles for electrons (**a**) and ions (**b**) for all plasma radii as used in NTSS (for the results shown in Fig. **5d** and **i**). Blue refers to the lower mirror case, red to the higher mirror case. The error band result from error propagation of the profile uncertainties.

Supplementary Fig. 2 shows the thermal transport coefficients as obtained by the energy convolution of $D_{11}^{\star}$ [36] for the temperatures, densities and radial electric field given at each radial position of the plasma:

$$D_{22}^{nc} = L_{22} - \frac{3}{2}L_{21}$$

$$D_{21}^{nc} = L_{21}$$

with (1) $$L_{ij} = \frac{2}{\sqrt{\pi}}\int_0^{\infty} dK\sqrt{K}\exp(-K)\, D_{11}^{\star}(K)\, D_{11}^{p} h_i h_j,\ h_1 = 1, h_2 = K$$

and $K = (m\mathrm{v}^2/2)/T$ and $D_{11}^{p} = \pi/4\left(\mathrm{v}_\mathrm{d}^2\mathrm{R}\right)/(\mathrm{v}\iota)$ the mono-energetic transport coefficient of the plateau regime (used in the normalization of $D_{11}^{\star}$). $\mathrm{v}_\mathrm{d} = \mathrm{mv}^2/(2\mathrm{qBR})$ is a radial drift velocity of

a particle with charge q. In order to estimate the range of K values which make the predominant contribution to transport (e.g. gray shaded area in Supplementary Fig. 1), the integrand of Eq. (1) is maximized. For energy transport this leads to largest contributions at K values well in excess of one.

The error bands reflect the influence of uncertainties in the profiles and Z_{eff} on the values of the thermal transport coefficients. In the core region ($E_r > 0$), the ion transport coefficients (Supplementary Fig. **2b**) are smaller than those of the electrons (Supplementary Fig. **2a**). At the same time, the gradients of the ions are also smaller than those of the electrons. Therefore, the ion contributions of the neoclassical energy fluxes are smaller than the dominating electron contributions (cf. Fig. **6b** and **e** in the main paper). The electron energy transport coefficients (Supplementary Fig. **2a**) match for both configurations (except for the small region of E_r/vB =0 in which $1/\nu$ transport is of relevance leading to larger transport coefficients in the higher-mirror case). Since also the plasma profiles are very similar (cf. Fig. 5), it can be concluded from the transport coefficients that the neoclassical contribution to the energy transport (Figs. 6**b** and **e**) is also very similar for the two magnetic configurations discussed in this paper. Since radiation and signals qualitatively indicating neutral particle fluxes are not different either, the similarity of neoclassical transport allows for the conclusion that also anomalous transport is not affected by the configuration change.

Supplementary Tab. 1 summarizes the W7-X confinement data shown in Fig. 4. The experimental confinement time was derived from the profiles as shown in Fig. 5. Uncertainties in the experimental confinement time τ_E include uncertainties in the profiles and Z_{eff}. The heating power and line averaged density correspond to the waveforms shown in Fig. 3 (with a chord length of L = 1.3 m). Errors in the mean density and the heating power are used to estimate the uncertainties of τ_{ISS04}.

Case	Heating power (MW)	Mean plasma density (m^{-3})	τ_E (ms)	τ_{ISS04} (ms)
*Lower mirror, higher power	1.07±0.11	0.91±0.09	122± 24	139±16
*Lower mirror, lower power	0.56±0.06	0.76±0.08	137± 27	187±23
$^{+}$Higher mirror, higher power	1.03±0.10	0.99±0.10	124± 25	151±17
$^{+}$Higher mirror, lower power	0.58±0.06	0.89±0.09	157± 31	203±24
*Best τ_E/ τ_{ISS04} (OP1.1)	3.80±0.38	2.73±0.27	128± 25	117±14

Supplementary Tab. 1| Energy confinement times in the first operation phase of W7-X.

Further scaling parameters for the configurations (*lower mirror, $^{+}$higher mirror) are summarized in Supplementary Tab. 2.

For the reference confinement time τ_{ISS04}, the ISS04 scaling expression [25].

$$\tau_{ISS04} = 0.134 a^{2.28} R^{0.64} P^{-0.61} n^{0.54} B^{0.84} \iota_{2/3}^{0.41}$$

was evaluated with the minor radius a, the major radius R, the mean magnetic field B and the rotational transform $\iota_{2/3}$ taken at 2/3 of the normalized plasma radius r_{eff}/a. Values of these parameters were calculated with VMEC calculations and are summarized in the supplementary Tab. 2. As for Ref. [25], uncertainties in the rotational transform minor radius and major radius are not considered. For the specific case discussed in the main article, the errors in the minor radius and the major radius is expected to be smaller than for other cases in the ISS04 database, since the plasma volume is well defined by limiters.

Case	rotational transform at 2/3 of the plasma radius $\iota_{2/3}$	Magnetic field B (T)	Minor radius a (m)	Major radius R (m)
*Lower mirror	0.814	2.414	0.491	5.514
$^{+}$Higher mirror	0.843	2.365	0.497	5.488

Supplementary Tab. 2| Confinement time scaling parameters for W7-X limiter configurations. The specific values are results from VMEC calculations also used for coordinate transformations (cf. Methods section).